Tropical Cyclone Gale Wind Radii Estimates for the Western North Pacific

CHARLES R. SAMPSON

Naval Research Laboratory, Monterey, California

EDWARD M. FUKADA AND JOHN A. KNAFF

NOAA/Center for Satellite Applications and Research, Fort Collins, Colorado

BRIAN R. STRAHL

Joint Typhoon Warning Center, Pearl Harbor, Hawaii

MICHAEL J. BRENNAN

NOAA/National Hurricane Center, Miami, Florida

TIMOTHY MARCHOK

NOAA/Geophysical Fluid Dynamics Laboratory, Princeton, New Jersey

(Manuscript received 9 November 2016, in final form 9 February 2017)

ABSTRACT

The Joint Typhoon Warning Center's (JTWC) forecast improvement goals include reducing 34-kt (1 kt = 0.514 m s^{-1}) wind radii forecast errors, so accurate real-time estimates and postseason analysis of the 34-kt wind radii are critical to reaching this goal. Accurate real-time 34-kt wind radii estimates are also critical for decisions regarding base preparedness and asset protection, but still represent a significant operational challenge at JTWC for several reasons. These reasons include a paucity of observations, the timeliness and availability of guidance, a lack of analysis tools, and a perceived shortage of personnel to perform the analysis; however, the number of available objective wind radii estimates is expanding, and the topic of estimating 34-kt wind radii warrants revisiting. In this work an equally weighted mean of real-time 34-kt wind radii objective estimates that provides real-time, routine operational guidance is described. This objective method is also used to retrospectively produce a 2-yr (2014–15) 34-kt wind radii objective analysis, the results of which compare favorably to the postseason National Hurricane Center data (i.e., the best tracks), and a newly created best-track dataset for the western North Pacific seasons. This equally weighted mean, when compared with the individual 34-kt wind radii estimate methods, is shown to have among the lowest mean absolute errors and smallest biases. In an ancillary finding, the western North Pacific basin average 34-kt wind radii calculated from the 2014–15 seasons are estimated to be 134 n mi (1 n mi = 1.852 km), which is larger than the estimates for storms in either the Atlantic (95 n mi) or eastern North Pacific (82 n mi) basins for the same years.

1. Introduction

Estimating the structure of the tropical cyclone (TC; see Table 1 for this and other key acronyms used in this paper) wind field is a critical part of the forecast process at U.S. TC forecast centers. These estimates include the maximum extent of the 34-kt (1 kt = 0.514 m s^{-1}), 50-kt, and 64-kt winds in compass quadrants (northeast, southeast, southwest, and northwest) surrounding the TC, which are collectively known as the "wind radii." These wind thresholds are also often referred to as gale-force, destructive,[1] and hurricane-force winds,

Corresponding author e-mail: Buck Sampson, buck.sampson@nrlmry.navy.mil

[1] The 50-kt winds are referred to as destructive winds by the Department of Defense, the basis for Tropical Cyclone Conditions of Readiness (TC-CORS) at DoD installations (Sampson et al. 2012).

DOI: 10.1175/WAF-D-16-0196.1

TABLE 1. List of key acronyms used in this paper.

AMSU	Advanced Microwave Sounding Unit
AOR	Area of responsibility
ATCF	Automated Tropical Cyclone Forecast System
AVNO	Global Forecast System model radii
CIRW	Cooperative Institute for Research in the Atmosphere CIRA wind radii estimates
CPHC	Central Pacific Hurricane Center
DVRK	Dvorak wind radii
GFDT	Geophysical Fluid Dynamics Laboratory model radii
HWRF	Hurricane Weather Research and Forecasting Model radii
JTWC	Joint Typhoon Warning Center, Pearl Harbor, HI
MAE	Mean absolute error
NWP	Numerical weather prediction
OBTK	Objective R34, an equally weighted average of R34 estimates
NHC	National Hurricane Center, Miami, FL
R34	Radii of 34-kt (15 m s^{-1}) winds. Also known as gale-force wind radii
TC	Tropical cyclone

respectively. An intense TC can require up to 12 estimates (four quadrants for each of the three radii thresholds), so the production of these estimates in real time can become a time-consuming task. However, these wind radii estimates are important to numerical weather prediction (NWP), decision aids, and end users. Since the operational units for wind radii distance and wind speeds are nautical miles (n mi; 1 n mi = 1.852 km) and knots, respectively, these units will be used for the remainder of this paper.

The real-time wind radii estimates are used to initialize NWP models (Tallapragada et al. 2015; Kurihara et al. 1993; Bender et al. 2016, 2017, manuscript submitted to *Wea. Forecasting*) and have been found to be of benefit. For example, Kunii (2015) found that the inclusion of wind radii data helped improve TC track forecasts in the Japan Meteorological Agency operational mesoscale model. Also, Marchok et al. (2012) showed that modifying the initial 34- and 50-kt wind radii in the Geophysical Fluid Dynamics Laboratory hurricane model had a significant impact on intensity forecasts. Finally, Wu et al. (2010) found significantly improved evolution of TC structure in the Weather Research and Forecasting Model during vortex initialization by assimilating wind radii information using an ensemble Kalman filter.

The real-time wind radii estimates are also used as inputs to decision aids such as the National Hurricane Center (NHC) wind speed probabilities (DeMaria et al. 2013a), storm surge forecasts (NHC 2016), wave forecasts (Sampson et al. 2010), modeling of potential infrastructure damages (e.g., Quiring et al. 2014), wind and wave/surge damage potential (Powell and Reinhold 2007), and Department of Defense danger swaths and Tropical Cyclone Conditions of Readiness (see Sampson et al. 2012). Also, the postseason reanalysis of wind radii, which make up part of the ''best tracks'' (NHC 2016) are used as ''ground truth'' to develop guidance that includes satellite-based estimates of wind radii/surface winds (Magnan 1998; Demuth et al. 2004, 2006; Mueller et al. 2006; Kossin et al. 2007; Knaff et al. 2011; Knaff et al. 2016; Dolling et al. 2016), the wind radii climatology and persistence model (Knaff et al. 2007), and real-time wind radii consensus forecasts (Sampson and Knaff 2015).

Wind radii poststorm analysis, or ''best tracking,'' has only been performed routinely at NHC since 2004, and only includes TCs in the North Atlantic, eastern North Pacific, and central North Pacific basins.[2] These wind radii best tracks are saved in the databases of the Automated Tropical Cyclone Forecast System (ATCF; Sampson and Schrader 2000). Although these best-track wind radii are used as ground truth, the errors in the best-track wind radii (specifically the 34-kt wind radii) have been estimated to be as high as 10%–40% (Knaff and Harper 2010; Landsea and Franklin 2013; Knaff and Sampson 2015), depending on the quality and quantity of the available observational data. For example, if aircraft, ship, and/or surface station reports are available in proximity to the TC or if there is a complete scatterometer pass over the TC, these data sources would provide higher confidence in the estimates.

The Joint Typhoon Warning Center (JTWC) is the organization responsible for forecasting TCs for U.S. interests in the western North Pacific, the Indian Ocean, and the entire Southern Hemisphere, a very large area of responsibility (AOR) that lacks a defined off season. In addition, there has traditionally been a dearth of surface wind data, wind radii estimates, and guidance for performing the task of poststorm wind radii analysis. Given these factors, JTWC has historically focused on only TC track and intensity postseason analysis and verification. However, with track and intensity forecasts continuing to improve [see Elliott and Yamaguchi (2014) and DeMaria et al. (2014), respectively], a much greater emphasis is being placed on improving wind radii estimates and forecasts. This accentuates the need for high quality wind radii estimation/forecast tools and postseason wind radii best tracks to validate such techniques.

[2] Best tracks for the central North Pacific basin, including wind radii, are provided by the Central Pacific Hurricane Center (CPHC) in Honolulu, Hawaii.

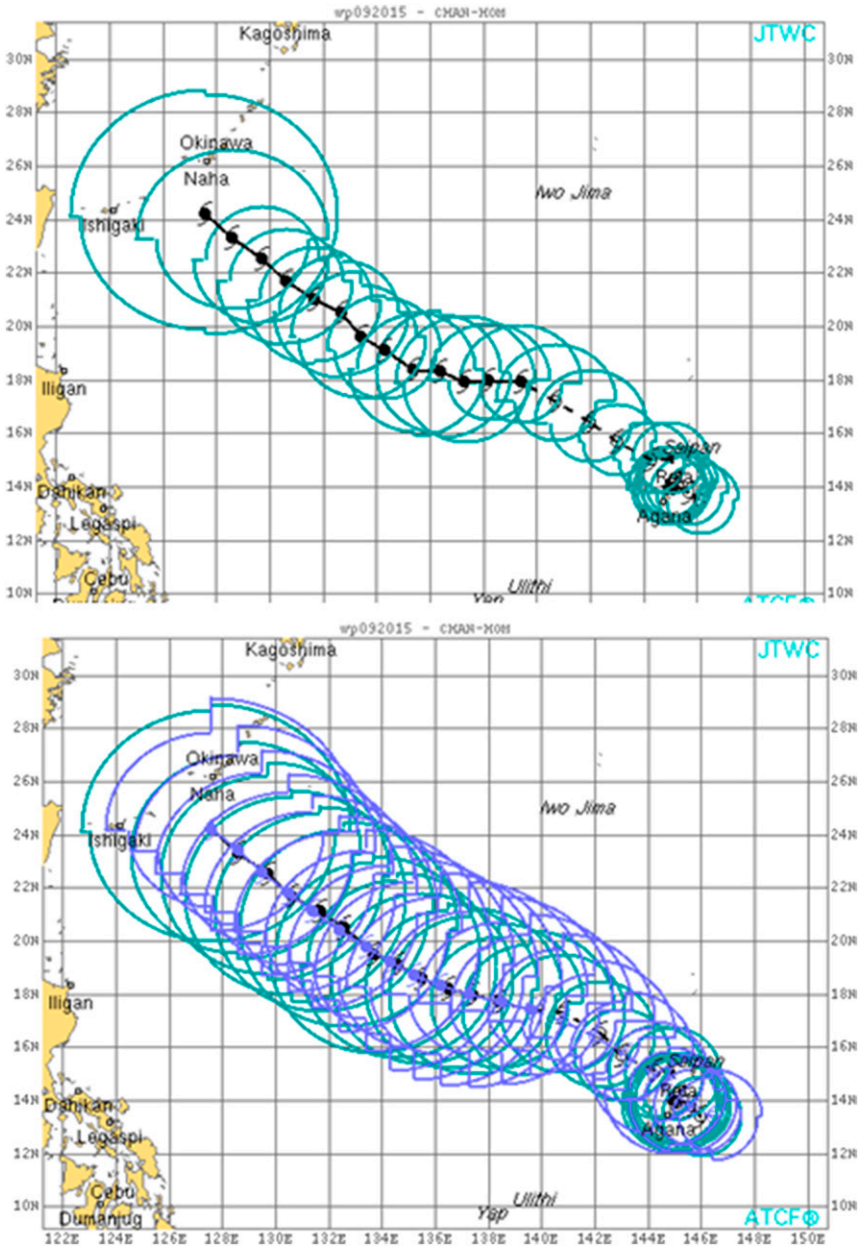

FIG. 1. JTWC (top) real-time and (bottom) postseason-analyzed 34-kt wind radii estimates from our objective technique (blue) and subjective analysis (green) for the 5 days leading up to Chan-Hom (ninth TC of the 2015 western North Pacific season) passing south of Okinawa.

An example of the importance of accurate 34-kt wind radii analyses and forecasts to U.S. Department of Defense operations is seen in the approach of Typhoon Chan-Hom (2015) toward Okinawa, Japan. The 34-kt wind radii (R34, hereafter) were analyzed between approximately 90 and 130 n mi for days preceding Chan-Hom's passage near the island. During this time, observations, including multiple scatterometer passes, failed to provide coverage over the TC's circulation. Short-term forecasts were likewise on the order of 100 n mi since they were largely based on persistence. Within 24 h of Chan-Hom's closest point of approach to Okinawa, the R34 estimates doubled in size (Fig. 1) after new scatterometer data indicated that earlier JTWC R34 analyses and forecasts were approximately 90 n mi too small. This sudden increase in R34 resulted in a short lead time for base preparations, despite accurate track forecasts and high-biased intensity forecasts. Similar discontinuities have been seen in other real-time R34

estimates, since R34 values are often left unchanged when new observational data are unavailable. Given that wind radii analyses are important for both end users and decision aids, we need to find ways to address shortcomings in analyzing R34.

There are several new and operationally available satellite-based wind radii estimates (Knaff et al. 2011; DeMaria et al. 2013b; Dostalek et al. 2016; Knaff et al. 2016) that have reasonably low mean R34 errors. Also, NWP modeling groups are trying to address TC wind structure issues as discussed by Harr and Kitabatake (2015 and related reports). Cangialosi and Landsea (2016; see their Fig. 5) showed that several NWP models provided skillful R34 forecasts for 2008–12 Atlantic TCs when compared with the highest quality wind radii estimates (i.e., those with coincident aircraft reconnaissance), a finding confirmed in a larger and more recent dataset in Sampson and Knaff (2015). The combination of improved NWP model skill, more numerous satellite-based estimates, and tools to efficiently view these estimates has enabled the creation of higher quality R34 estimates for use at the JTWC and elsewhere, and that effort is described in the remainder of this paper.

The goals of this work are to 1) create and describe an objective method that provides R34 estimates for use in real-time and postseason analyses, 2) demonstrate that this method is valid by comparing its results with NHC best tracks, and 3) demonstrate its potential capabilities and use in the western North Pacific.

The datasets and processes used to create objective and postseason subjective analyses of R34 are described in section 2. In section 3 we evaluate our objective analyses against NHC best-track R34 analyses with coincident scatterometer passes, and then evaluate our objective analysis against a newly created 2014–15 western North Pacific R34 best-track dataset. In section 4 we summarize our findings on the performance of the R34 objective guidance and the newly created R34 best tracks; we then provide suggestions for their use.

2. Data and methods

The best-track dataset used in this study includes all 2014 and 2015 Atlantic, eastern North Pacific, and western North Pacific TCs. However, the process followed to produce these best tracks is difficult and subjective and can vary among forecast organizations and even forecasters at the same forecast center. To provide the reader additional information about how the wind radii best tracks used here were created, the R34 best-track methods used at NHC and JTWC are documented in appendixes A and B, respectively. R34 is defined as the radius of the maximum extent of 34-kt winds in compass directions surrounding TCs that have intensities (i.e., maximum sustained 10-m 1-min winds) of 34 kt ($17\,m\,s^{-1}$) or greater. As discussed earlier, NHC has performed postseason analysis of the wind radii since 2004, while the process is still under evaluation at JTWC. As in previous research efforts (e.g., Sampson and Knaff 2015), this study will concentrate on R34 verification since R34 cases are the most-often analyzed and likely the best-observed wind radii. Analysis of scatterometry is one of the best methods for constructing wind radii analyses around TCs. Bentamy et al. (2008), Brennan et al. (2009), and Chou et al. (2013) suggest that scatterometer winds can be used specifically for R34 analysis. The scatterometer passes cover large areas of the ocean and generally provide high quality estimates of wind speeds less than approximately 50 kt when they are available. Scatterometry is thus considered a high quality metric for R34. The authors are aware of the potential for larger errors in the R34 best-track analyses that are in the NHC data (see Knaff and Sampson 2015; Knaff et al. 2006) and used here as "ground truth." To address this issue, the authors limit their use of NHC R34 best tracks to times with coincident scatterometer fixes (±3 h) in the ATCF database.

To form our objective estimate or objective best track (OBTK) of initial wind radii, three satellite-based and three model-based estimates are combined using an equally weighted average. The number of input estimates is allowed to vary between one and six, depending on their availability. Combining independent estimates and forecasts to form an average has long been shown to reduce uncertainty and errors (see Student 1908; Bates and Granger 1969). The satellite-based estimates are somewhat independent in that they use different remotely sensed data from different platforms. The first satellite method constructs wind radii estimates based on the Advanced Microwave Sounding Unit (AMSU) instrument that is flown on NOAA and European satellites. The wind radii retrievals from AMSU (specifically AMSU-A) are based on retrievals from a statistical approach (Goldberg et al. 2001) and the Microwave Integrated Retrieval System (Boukabara et al. 2011) using an algorithm described in Demuth et al. (2006). The second satellite method uses Dvorak (1984) satellite intensity, position, and motion estimates along with matching digital storm infrared (IR) imagery and a climatological estimate of the radius of maximum winds to create estimates of wind radii. These Dvorak wind radii (DVRK) are described in detail in Knaff et al. (2016). The third and final satellite-based estimate is the National Environmental Satellite, Data, and Information Service operational multisatellite TC surface wind analysis developed at the Cooperative Institute for Research in the Atmosphere, described in Knaff et al. (2011) and referred to herein as CIRW. The

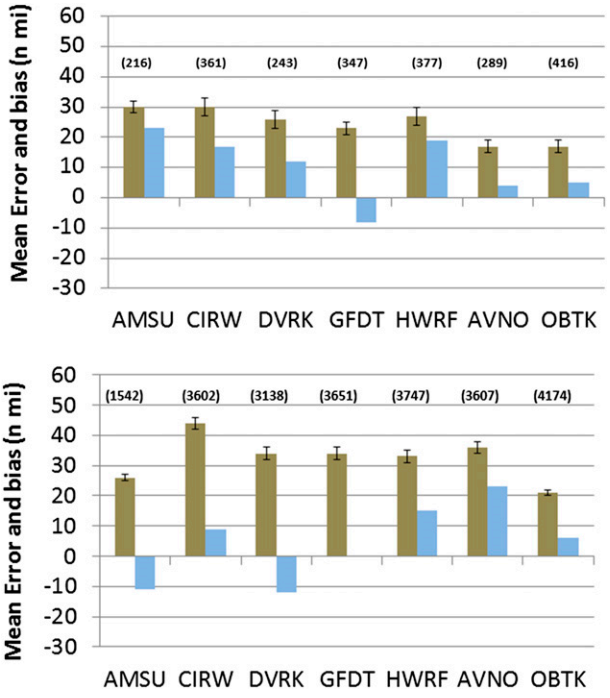

FIG. 2. The 34-kt wind radii fix mean errors (brown) and biases (blue) relative to (top) NHC 2014–15 best tracks coincident with scatterometer passes in the Atlantic and eastern North Pacific, and (bottom) for the entire western North Pacific 2014–15 JTWC best-track dataset. Standard error is shown as black bars on means, and the number of cases is shown in parentheses.

satellite-based technique estimates are supplemented by 6-hourly R34 model forecasts from the Marchok tracker (Marchok 2002). The R34 forecasts are currently limited to the Global Forecast System model, the Hurricane Weather Research and Forecasting Model, and the Geophysical Fluid Dynamics Laboratory Hurricane model. These three NWP model-based estimates are hereafter referred to as AVNO, HWRF, and GFDT, respectively. To be used in the equally weighted average, individual estimates must be available ±3 h from the synoptic times (0000, 0600, 1200, and 1800 UTC). A three-point center-weighted filter is run 10 times on the resultant R34 OBTK to smooth the R34 values through time. This smoothing is especially important for the times when a TC's intensity is near 35 kt or the TC is becoming extratropical, as it provides stability in the R34 estimates in time.

To calculate verification statistics, values of R34 in each quadrant are compared with the final best-track values for each estimate. The occurrence of zero-valued wind radii in one or more of the storm quadrants introduces an added complication when verifying wind radii. Zero-valued R34 values typically occur when the maximum wind speeds in storms are near the 35-kt intensity threshold or when storm translation speeds are large (i.e., greater than $8\,m\,s^{-1}$). For this study the following verification strategy is adopted: if any of the quadrants in the best track have nonzero wind radii, all quadrants for that case and lead time are verified. Using this strategy, we average the error values from quadrants with nonzero wind radii to form a single measurement of the mean absolute error (MAE) and bias.

To evaluate the ability of the OBTK R34 estimates to discriminate the occurrence of R34 and to complement the MAE and bias statistics, the availability rate and false alarm rate are also discussed. We define the mean bias as the average of the estimated value minus the ground truth. We also define the availability rate differently than a probability of detection in that probability of detection only applies when the guidance is available. Availability rate is more applicable to our operational forecast problem because it is measured against all instances of R34 in the best track. Therefore, the availability rate can be much lower than the probability of detection if the guidance is only available intermittently. The false alarm rate is based on whether or not a quadrant had a nonzero R34 value.

To keep the verification brief, we present the statistics for combined quadrants (i.e., the errors in all quadrants are averaged). Errors are also calculated in homogeneous sets (i.e., they all include the same cases), and the results of the verification will be presented in the next section.

3. Results

As discussed earlier, the authors chose to evaluate OBTK against NHC best-track estimates when scatterometer fixes were available in the ATCF database. This methodology was chosen in an effort to use many of the higher quality estimates of R34.The top panel in Fig. 2 shows an evaluation of a 2-yr (2014 and 2015) sample of the six consensus members R34 estimates and OBTK, all coincident with scatterometer passes that have been subjectively analyzed (Brennan et al. 2009) within NHC's areas of operation. Table 1 again provides expansions for acronyms used in Fig. 2.

For the eastern North Pacific and Atlantic combined data shown in the top panel in Fig. 2, we can discern that the MAEs of all the methods range between 17 and 30 n mi, which is approximately 20%–30% of the value of the mean radii for those basins. Most of the methods have a high bias, indicating that their estimated R34 is generally too large. The OBTK has among the lowest MAEs and mean biases when compared with the six consensus members.

One unexpected finding in this evaluation is that the mesoscale model (GFDT and HWRF) estimates have similar errors and biases when compared with the other estimates, even though these models assimilate the real-time

TABLE 2. The 2014 and 2015 best-track climatological mean 34-kt wind radii, mean error, and bias in the real-time subjective estimates from the forecasters.

Basin	No. of cases	Best-track mean R34 (n mi)	Real-time estimate MAE (n mi)	Real-time estimate bias (n mi)
Atlantic	974	95	6	−2
Eastern North Pacific	3070	82	3	0
Western North Pacific	3707	134	30	−27

NHC wind radii estimates. The CIRW and AVNO both assimilate scatterometer winds, and AVNO also appears to have the lowest MAE and bias compared with the best-track estimates coincident with scatterometer passes (Fig. 2, top). The interplay between best-track R34 uncertainty, interdependence of the estimates, and ground truth coincident with scatterometer passes presents issues that will not be addressed in this study.

The bottom panel in Fig. 2 shows the performance of the same R34 estimates and the equally weighted mean for the newly created 2014–15 western North Pacific best tracks. The MAE values in the estimates are higher than in the NHC dataset, ranging from approximately 21 to 42 n mi, but they still represent approximately 20%–30% of the mean radius for the dataset in that basin (see Table 2). The biases range from −12 to 21 n mi and are not consistent with the biases in the NHC data. The western North Pacific dataset is not limited to best-track data with coincident scatterometer passes, and in this sample the AVNO estimates are now on par with the other estimates. The OBTK has the lowest MAE and a small positive bias comparable to its bias in the NHC dataset. An inspection of the OBTK values for both datasets indicates that these mean R34 estimates generally vary slowly with time compared with the individual estimates, which is a desirable feature for maintaining consistency in operational analysis and forecasting. The standard deviation of the OBTK errors (14 n mi) provides one measure of R34 uncertainty.

Another benefit of the OBTK is that it is designed to have nearly 100% availability (Fig. 3). An availability rate of less than 100% is expected for each of the individual estimates and is somewhat problematic for forecasters who need guidance for all their official R34 estimates. The AMSU-based R34 estimates are reasonably accurate (see Fig. 2), but their availability rate is limited to approximately 35% of the time as a result of the geometry of polar satellite orbit overpasses and a 1400-km effective swath. The other individual estimate availability rates are between 70% and 90%, and the OBTK availability is nearly 98% for this dataset.

The number of cases where observed radii do not exist (857) is about 20% as large as the number of cases where R34 exists. The OBTK false alarm rate is 50% (423 out of 857 cases). In operational forecasting, a high false alarm rate is not necessarily a liability since the operational forecast intensity (35 kt or greater for our sample) determines whether or not the forecaster creates real-time R34 estimates. The authors also consider a high false alarm rate to be a benefit since it could also provide advanced guidance of TC structure when the TC reaches 35 kt—noting that the uncertainty of the intensity analysis estimates is on the order of 10 kt (Landsea and Franklin 2013; Torn and Snyder 2012).

We have made no effort to correct biases in or unevenly weight the individual estimates in the OBTK since it is our opinion (and others, e.g., Kharin and Zwiers 2002; Weigel et al. 2010; DelSole et al. 2013) that assigning weights to the individual estimates is difficult, especially when the accuracy of the individual estimates is changing with time (e.g., the NWP model estimates should improve as the NWP models improve). Also, an inspection of the entire dataset indicates that the OBTK estimates are more consistent with time when more of the individual estimates are available. When the number of the individual estimates is low (e.g., at the beginning or near the end of a TC life cycle when there may only be between one and three estimates available), the OBTK R34 estimates can change rapidly with time. This is an undesirable feature for operational forecasting, so additional R34 estimates (e.g., from other NWP

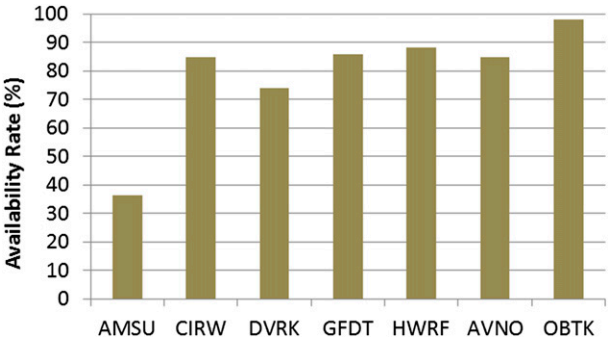

FIG. 3. Wind radii estimate availability based on 4251 best-track radius estimates for the JTWC western North Pacific 2014–15 seasons.

models and from other satellite-databased algorithms) would likely improve the operational utility of the OBTK. Also, increasing the number of independent estimates (e.g., estimates from different satellite platforms) should also improve OBTK performance, similar to findings in efforts to improve TC track and intensity forecast guidance (see Goerss et al. 2004; Sampson et al. 2008).

4. Conclusions and recommendations

In this paper we have evaluated six individual estimates of R34 against NHC best tracks (described in appendix A) coincident with scatterometer passes from 2014 and 2015 and found that the estimates had errors that ranged between 17 and 30 n mi, and had biases that ranged between −8 and 23 n mi. We then formed an equally weighted mean of these estimates (OBTK), and found its performance to be among the best in terms of both error and bias when compared with the NHC best-track estimates.

We then applied our algorithm to the western North Pacific 2014 and 2015 seasons to create higher quality R34 estimates for use in reanalyzing the JTWC R34 estimates. In appendix B we performed a double-blind study to create a subjective best track of R34 on one eastern North Pacific TC (Blanca from the 2015 season) and found that our independent R34 estimates compared favorably with those of the NHC. We then created a 2-yr subjective reanalysis (best track) of R34 for the western North Pacific. We found that the average R34 value for our western North Pacific best track is 134 n mi, which is much higher than the average of real-time western North Pacific estimates (103 n mi). For comparison, the average R34 is 95 n mi in the Atlantic best tracks and 82 n mi in the eastern North Pacific best tracks for the same years. The OBTK mean error relative to some of the highest quality NHC R34 estimates (those coincident with scatterometer passes) is 17 n mi, and the standard deviation (a measure of uncertainty) is 14 n mi. Uncertainty estimates for best-track radii without coincident scatterometer passes are expected to be higher.

Now that we have a way of producing higher quality estimates of R34 in the western North Pacific, we can apply our methodology to other years and other basins to create a higher quality best-track R34 record for use in climatology studies (e.g., Wu et al. 2015). This higher quality record can also be used to (re)develop guidance such as the wind radii climatology and persistence model (Knaff et al. 2007), wind radii consensus aids (see Sampson and Knaff 2015), and consensus-based error estimates similar to those created for intensity in Goerss and Sampson (2014). These guidance improvements would then be available to operational forecasters and have implications for end-user products such as those discussed in the introduction. The OBTK could possibly be improved by the addition of more quality wind radii guidance. Some potential methods include the IR-based method discussed in Dolling et al. (2016), Global Navigation Satellite System reflectometry methods (Ruf et al. 2016) and L-band microwave-based methods discussed in Reul et al. (2016) and Meissner et al. (2014). These methods will be investigated as OBTK members in the near future.

Finally, there is hope of improving the estimates of the 50- and 64-kt wind radii. Not only is there evidence of dependence of these radii on the 34-kt wind radii (see Knaff et al. 2016), but there are already several independent satellite-based estimates of these radii that could be used to develop this capability.

Acknowledgments. The authors would like to acknowledge the staff at NHC and JTWC, the NOAA GOES and GOES-R program offices for support of TC structure studies, and the important behind-the-scenes efforts of Ann Schrader and Mike Frost. Careful reading of reviewers and managers from several agencies is also acknowledged. Specifically, we thank Chris Landsea, Ed Rappaport, and Todd Kimberlain of NHC for comments on previous versions of this manuscript. This publication was graciously funded by the Office of Naval Research, Program Elements 0602435N. The views, opinions, and findings contained in this report are those of the authors and should not be construed as an official National Oceanic and Atmospheric Administration or U.S. government position, policy, or decision.

APPENDIX A

NHC 34-kt Wind Radii Postanalysis

At the National Hurricane Center (NHC), 34-kt wind radii are reanalyzed as part of the poststorm "best track" analysis of the tropical cyclone (and its post-tropical stage, if applicable). These analyses are valid at 0000, 0600, 1200, and 1800 UTC, and this reanalysis also includes the location of the TC center, its intensity, and 50- and 64-kt wind radii.

Available data for postanalysis in NHC's AOR include in situ ship, buoy, and land observations; flight-level winds and stepped-frequency microwave radiometer surface wind speed measurements from aircraft reconnaissance; dropwindsondes from aircraft; scatterometer winds; and estimates of wind radii from

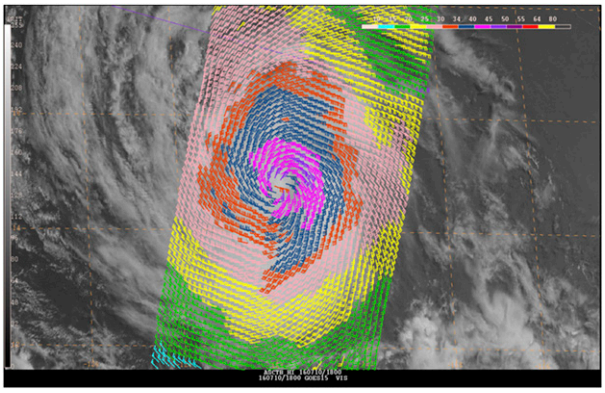

FIG. A1. Winds (kt) from an ASCAT-B overpass of eastern Pacific Hurricane Celia at 1808 UTC 10 Jul 2016 overlaid with GOES-West visible imagery in the N-AWIPS display system at NHC. Winds above 34 kt are shown in dark blue.

microwave sounders such as AMSU. The amount of data available for each TC and at various times within the same TC's life cycle varies widely. For example, aircraft reconnaissance data are only available in about 30% of Atlantic TCs (mostly in the western part of the basin), and only rarely in TCs in the eastern North Pacific basin (typically when hurricanes threaten the coast of Mexico). Even when aircraft data are available, the point data available along the aircraft flight path typically sample only about 2% of the TC's wind field in a full "alpha" pattern through the cyclone. Scatterometers can provide better spatial coverage of winds, but passes are at most available only twice a day from low-Earth satellites in polar orbit at the low and midlatitudes where most TCs are found. There are also gaps between scatterometer data swaths, especially in the tropics, that can result in sampling only part of the TC wind field or total "misses" for multiple passes in a row. In situ surface observations are even more sporadic and are, typically, found close to major landmasses and islands, particularly in the western Atlantic basin. Most of the eastern North Pacific basin is completely devoid of in situ wind data apart from infrequent aircraft flights, as mentioned above, or occasional ship data.

The starting point for the reanalysis is the operational 34-kt wind radii that were made in real time by the duty hurricane specialist. Given that these real-time estimates are made under operational time constraints, and that most remotely sensed data have some temporal latency that results in a 1–3-h delay in the receipt of the data, the postanalysis process provides an opportunity to revisit the 34-kt wind radii in a

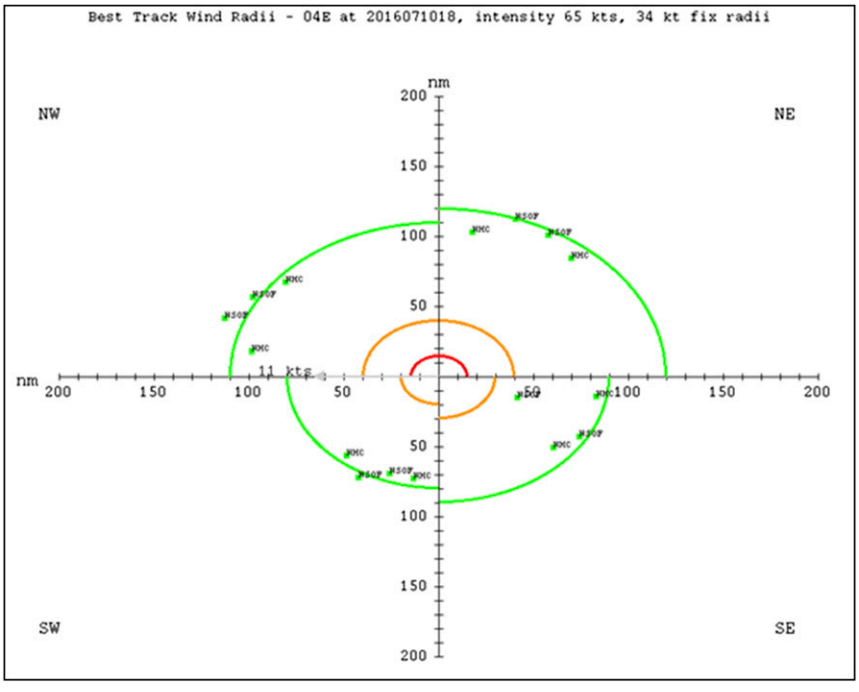

FIG. A2. Wind radii polar diagram from the ATCF showing best-track 34-kt wind radii in each quadrant (green arcs) and individual 34-kt wind radii fixes (green dots) in each quadrant for Hurricane Celia at 1800 UTC 10 Jul 2016. Also shown are arcs for 50- (orange) and 64-kt (red) wind radii. TC motion (W at 11 kt) is also shown. All distances are shown in n mi.

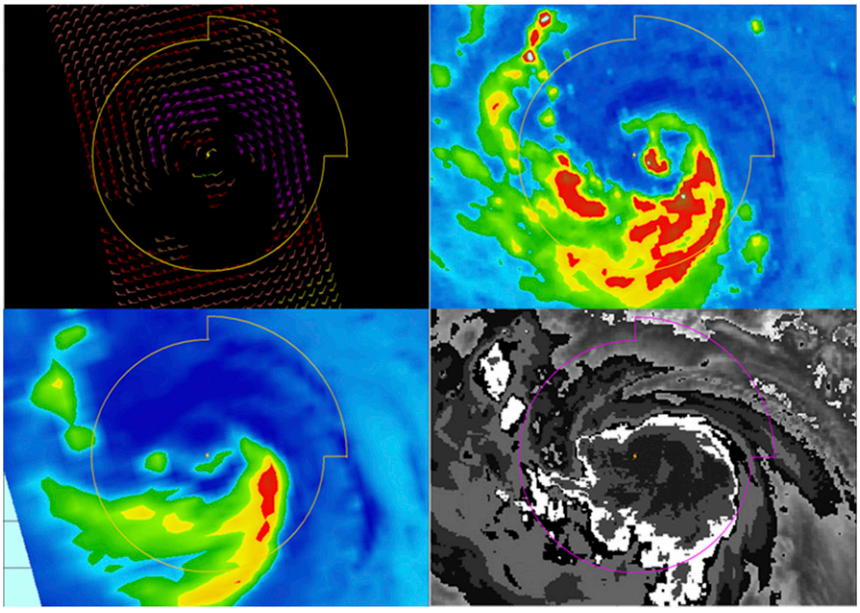

FIG. B1. Examples of the imagery used to determine 1200 UTC 6 Sep R34 estimates for Chan-Hom, the ninth TC of the JTWC western North Pacific 2015 season. (top left) Scatterometer imagery at 1141 UTC 6 Sep, (top right) 91-GHz imagery at 0949 UTC 6 Sep, (bottom left) 89-Ghz imagery at 1140 UTC 6 Sep, and (bottom right) enhanced infrared imagery at 1132 UTC 6 Sep. R34 postseason estimates are shown for comparison.

more holistic manner and with the benefit of having all the data available for the analysis. Given the uncertainty and often the lack of data involved in the analysis process, NHC currently rounds 34-kt wind radii in each quadrant to the nearest 10 n mi and tries to show bulk trends in the wind field that can be captured by the temporal resolution of a 6-h best track.

During the reanalysis process, all available data are used, with the most weight given to direct wind measurements from aircraft, scatterometry, and surface data. When there are large spatial gaps between the available data, such as in open-ocean storms, the analysis is typically anchored on available data, such as scatterometer passes, and the analysis at times between those observations is smoothed to fit the available data at the beginning and end of the period, taking into account intervening changes in the intensity, motion, and structure of the TC.

These data are viewed in a variety of platforms. Aircraft data, surface observations, and scatterometer data are available in the N-AWIPS software system, which allows the analyst to overlay the data together with geostationary satellite imagery and measure the wind radii directly (Fig. A1). Wind radii "fixes" are also entered into the ATCF database and are available for viewing both in text and graphical formats (Fig. A2).

APPENDIX B

JTWC 34-kt Wind Radii Postanalysis

JTWC real-time estimates of R34 in the western North Pacific are largely based on timely scatterometer passes, multiplatform satellite wind analyses, analysis of microwave and infrared imagery patterns, and occasional ship and station observations. Although routine aircraft reconnaissance operations ended in 1987, occasionally aircraft data are available to forecasters for TCs approaching Taiwan. When noted observations are unavailable in real time, the JTWC R34 estimates are generally persistence from prior estimates.

For the 2014–15 postseason R34 analyses, storm-following imagery (scatterometer winds, visible and IR imagery, and microwave imagery) was obtained from the Fleet Numerical Meteorology Center and the Naval Research Laboratory Tropical Cyclone Page website (Fig. B1). NWP 6-h forecasts of R34 from the Global Forecast System and Hurricane Weather Research Forecast System were obtained from the ATCF archive, as were AMSU-based and multiplatform-based wind radii estimates. Geophysical Fluid Dynamics Laboratory NWP model wind radii were obtained from reruns for both the 2014 and 2015 seasons. Dvorak wind radii estimates were computed postseason using the Naval

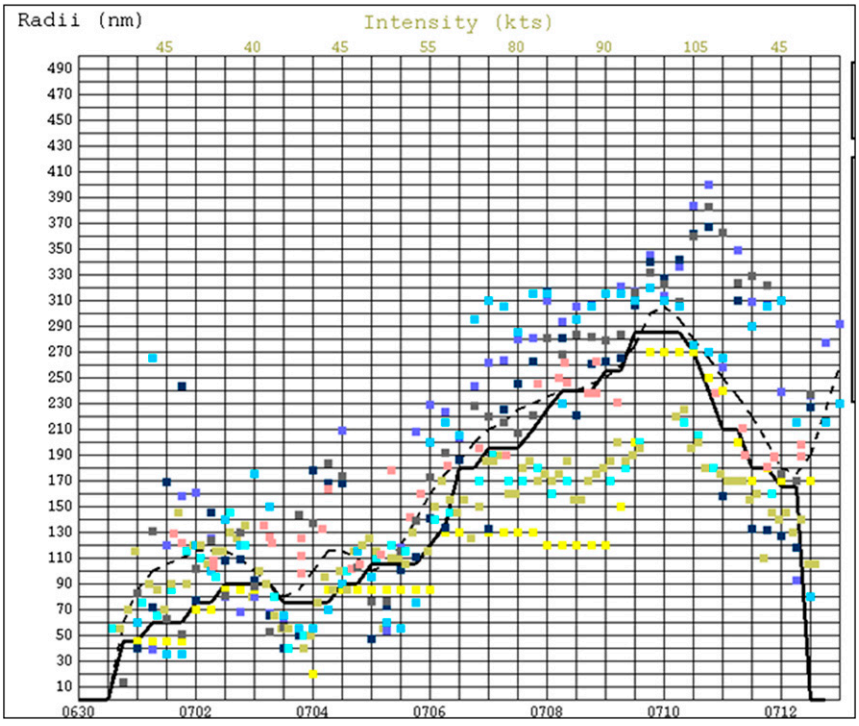

FIG. B2. Wind radii vs time plot for the northeastern quadrant of Chan-Hom. Yellow dots indicate real-time JTWC estimates, other dots indicate objective estimates, the dashed black line indicates the equally weighted average, and the red line indicates the postseason analysis.

Research Laboratory Tropical Cyclone Page imagery and the JTWC Dvorak estimates.

The position and intensity best tracks, already analyzed postseason, were taken from the ATCF archive and reviewed from start to finish. Then, noted imagery was overlaid onto JTWC real-time R34 estimates. JTWC real-time R34 estimates were compared with the OBTK described in the body of this paper and, when scatterometer imagery was unavailable, the members of OBTK were used as a baseline or first guess. Temporal

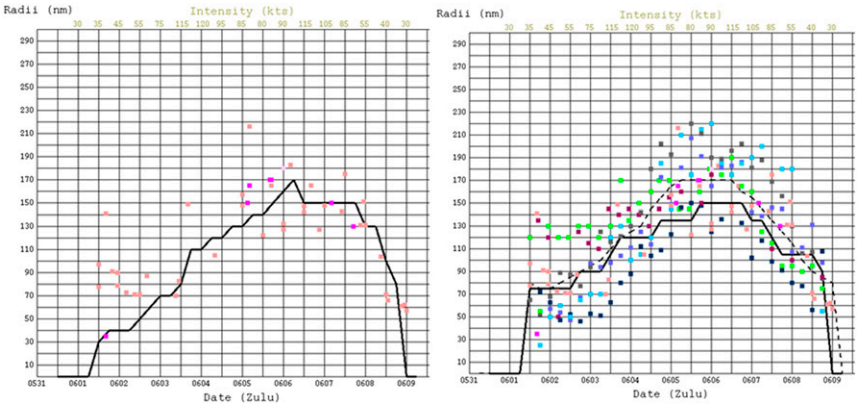

FIG. B3. (left) NHC 34-kt wind radii estimates (black line) through time for the northeastern quadrant in Blanca (ep022015) with scatterometer fixes (purple) and AMSU estimates (salmon). (right) NRL reanalysis of the same quadrant (solid black line) completed using objective estimates (multicolored dots) and an equally weighted average of the objective estimates (dashed line), scatterometer data, and other resources. In both plots, the observed intensity (kt) at 12-h intervals is indicated along the top of the plot in light green.

continuity in the estimates was also considered (see Fig. B2). As in the NHC procedure, R34 was determined for all intensities of 35 kt or greater. R34 was specified in increments of 15 n mi in order to minimize small and short-term fluctuations. For each R34 estimate, justifications were recorded in logs and saved in the ATCF archive.

Since the R34 postseason analysis at JTWC is a new effort, we were unsure of the quality of our reanalyzed R34 values, particularly given the sparsity of quality observational data. To validate the methods and processes, we ran a double-blind experiment using a fairly well-behaved tropical cyclone in the eastern North Pacific (Fig. B3). Using only the fixes and imagery available in the ATCF (no aircraft data and no estimates from NHC), we produced our own independent estimates of R34 for this TC. The results in Fig. B3, though anecdotal, show that our methodology provided estimates similar in size to those of the NHC postseason analysis. Differences do exist, as they do between the objective estimates and NHC best tracks. Most of the large differences are within the 20% (or 30 n mi) range. The largest differences are in the R34 estimates both at the beginning and end of the TC life cycle.

REFERENCES

Bates, J. M., and C. W. J. Granger, 1969: The combination of forecasts. *Oper. Res.*, **20**, 451–468, doi:10.1057/jors.1969.103.

Bender, M. A., M. J. Morin, K. Emanuel, J. A. Knaff, C. Sampson, I. Ginis, and B. Thomas, 2016: Impact of storm structure and the environmental conditions in the rapid intensification of Hurricanes Katrina and Patricia. *32nd Conf. on Hurricanes and Tropical Meteorology*, San Juan, PR, Amer. Meteor. Soc., 6D.2. [Available online at https://ams.confex.com/ams/32Hurr/webprogram/Paper293687.html.]

Bentamy, A., D. Croize-Fillon, and C. Perigaud, 2008: Characterization of ASCAT measurements based on buoy and QuikSCAT wind vector observations. *Ocean Sci.*, **4**, 265–274, doi:10.5194/os-4-265-2008.

Boukabara, S. A., and Coauthors, 2011: MiRS: An all-weather 1DVAR satellite data assimilation and retrieval system. *IEEE Trans. Geosci. Remote Sens.*, **49**, 3249–3272, doi:10.1109/TGRS.2011.2158438.

Brennan, M. J., C. C. Hennon, and R. D. Knabb, 2009: The operational use of QuikSCAT ocean surface vector winds at the National Hurricane Center. *Wea. Forecasting*, **24**, 621–645, doi:10.1175/2008WAF2222188.1.

Cangialosi, J. P., and C. W. Landsea, 2016: An examination of model and official National Hurricane Center tropical cyclone size forecasts. *Wea. Forecasting*, **31**, 1293–1300, doi:10.1175/WAF-D-15-0158.1.

Chou, K.-H., C.-C. Wu, and S.-Z. Lin, 2013: Assessment of the ASCAT wind error characteristics by global dropwindsonde observations. *J. Geophys. Res.*, **118**, 9011–9021, doi:10.1002/jgrd.50724.

DelSole, T., X. Yang, and M. K. Tippett, 2013: Is unequal weighting significantly better than equal weighting for multi-model forecasting? *Quart. J. Roy. Meteor. Soc.*, **139**, 176–183, doi:10.1002/qj.1961.

DeMaria, M., and Coauthors, 2013a: Improvements to the operational tropical cyclone wind speed probability model. *Wea. Forecasting*, **28**, 586–602, doi:10.1175/WAF-D-12-00116.1.

——, A. Schumacher, J. Dostalek, S. Longmore, L. Zhao, and L. Ma, 2013b: S-NPP microwave sounder-based TC products algorithm theoretical basis document. NOAA/NESDIS, 18 pp. [Available online at http://www1.ncdc.noaa.gov/pub/data/metadata/documents/C00937_Algorithm_Theoretical_Basis_Document_NTCP_v1.1.docx.]

——, C. R. Sampson, J. A. Knaff, and K. D. Musgrave, 2014: Is tropical cyclone intensity guidance improving? *Bull. Amer. Meteor. Soc.*, **95**, 387–398, doi:10.1175/BAMS-D-12-00240.1.

Demuth, J. L., M. DeMaria, J. A. Knaff, and T. H. Vonder Haar, 2004: Evaluation of Advanced Microwave Sounder Unit (AMSU) tropical cyclone intensity and size estimation algorithm. *J. Appl. Meteor.*, **43**, 282–296, doi:10.1175/1520-0450(2004)043<0282:EOAMSU>2.0.CO;2.

——, ——, and ——, 2006: Improvement of Advanced Microwave Sounding Unit tropical cyclone intensity and size estimation algorithms. *J. App. Meteor. Climatol.*, **45**, 1573–1581, doi:10.1175/JAM2429.1.

Dolling, K., E. A. Ritchie, and J. S. Tyo, 2016: The use of the deviation angle variance technique on geostationary satellite imagery to estimate tropical cyclone size parameters. *Wea. Forecasting*, **31**, 1625–1642, doi:10.1175/WAF-D-16-0056.1.

Dostalek, J., G. Chirokova, J. Knaff, S. Longmore, R. T. DeMaria, A. B. Schumacher, and C. Sampson, 2016: Recent and future updates to the operational, satellite-based tropical cyclone products produced at the Cooperative Institute for Research in the Atmosphere. *32nd Conf. on Hurricanes and Tropical Meteorology*, San Juan, PR, Amer. Meteor. Soc., 11C.7. [Available online at https://ams.confex.com/ams/32Hurr/webprogram/Paper293020.html.]

Dvorak, V. F., 1984: Tropical cyclone intensity analysis using satellite data. NOAA Tech. Rep. NESDIS 11, 45 pp. [Available online at ftp://satepsanone.nesdis.noaa.gov/Publications/Tropical/Dvorak_1984.pdf.]

Elliott, G., and M. Yamaguchi, 2014: Motion—Recent advances. Summary Rep. on Eighth Int. Workshop on Tropical Cyclones (IWTC-8), WMO, 44 pp. [Available online at http://www.wmo.int/pages/prog/arep/wwrp/new/documents/Topic1_AdvancesinForecastingMotion.pdf.]

Goerss, J. S., and C. R. Sampson, 2014: Prediction of consensus tropical cyclone intensity forecast error. *Wea. Forecasting*, **29**, 750–762, doi:10.1175/WAF-D-13-00058.1.

——, ——, and J. Gross, 2004: A history of western North Pacific tropical cyclone track forecast skill. *Wea. Forecasting*, **19**, 633–638, doi:10.1175/1520-0434(2004)019<0633:AHOWNP>2.0.CO;2.

Goldberg, M. D., D. S. Crosby, and L. Zhou, 2001: The limb adjustment of AMSU-A observations: Methodology and validation. *J. Appl. Meteor.*, **40**, 70–83, doi:10.1175/1520-0450(2001)040<0070:TLAOAA>2.0.CO;2.

Harr, P. A., and N. Kitabatake, 2015: Structure and structure change. *Eighth Int. Workshop on Tropical Cyclones*, Jeju Island, South Korea, WMO, T4. [Available online at http://www.wmo.int/pages/prog/arep/wwrp/new/documents/Topic4.pdf.]

Kharin, V. V., and F. W. Zwiers, 2002: Climate predictions with multimodel ensembles. *J. Climate*, **15**, 793–799, doi:10.1175/1520-0442(2002)015<0793:CPWME>2.0.CO;2.

Knaff, J. A., and B. A. Harper, 2010: Tropical cyclone surface wind structure and wind-pressure relationships. *Seventh Int. Workshop on Tropical Cyclones*, La Reunion, France, WMO, KN1. [Available online at https://www.wmo.int/pages/prog/arep/wwrp/tmr/otherfileformats/documents/KN1.pdf.]

——, and C. R. Sampson, 2015: After a decade are Atlantic tropical cyclone gale force wind radii forecasts now skillful? *Wea. Forecasting*, **30**, 702–709, doi:10.1175/WAF-D-14-00149.1.

——, C. Guard, J. Kossin, T. Marchok, C. Sampson, T. Smith, and N. Surgi, 2006: Operational guidance and skill in forecasting structure change. *Sixth Int. Workshop on Tropical Cyclones*, San Juan, Costa Rica, WMO, 160–184. [Available online at http://severe.worldweather.org/iwtc/document/Topic_1_5_John_Knaff.pdf.]

——, C. R. Sampson, M. DeMaria, T. P. Marchok, J. M. Gross, and C. J. McAdie, 2007: Statistical tropical cyclone wind radii prediction using climatology and persistence. *Wea. Forecasting*, **22**, 781–791, doi:10.1175/WAF1026.1.

——, M. DeMaria, D. A. Molenar, C. R. Sampson, and M. G. Seybold, 2011: An automated, objective, multisatellite platform tropical cyclone surface wind analysis. *J. Appl. Meteor. Climatol.*, **50**, 2149–2166, doi:10.1175/2011JAMC2673.1.

——, C. J. Slocum, K. D. Musgrave, C. R. Sampson, and B. Strahl, 2016: Using routinely available information to estimate tropical cyclone wind structure. *Mon. Wea. Rev.*, **144**, 1233–1247, doi:10.1175/MWR-D-15-0267.1.

Kossin, J. P., J. A. Knaff, H. I. Berger, D. C. Herndon, T. A. Cram, C. S. Velden, R. J. Murnane, and J. D. Hawkins, 2007: Estimating hurricane wind structure in the absence of aircraft reconnaissance. *Wea. Forecasting*, **22**, 89–101, doi:10.1175/WAF985.1.

Kunii, M., 2015: Assimilation of tropical cyclone track and wind radius data with an ensemble Kalman filter. *Wea. Forecasting*, **30**, 1050–1063, doi:10.1175/WAF-D-14-00088.1.

Kurihara, Y., M. A. Bender, and R. J. Ross, 1993: An initialization scheme of hurricane models by vortex specification. *Mon. Wea. Rev.*, **121**, 2030–2045, doi:10.1175/1520-0493(1993)121<2030:AISOHM>2.0.CO;2.

Landsea, C. W., and J. L. Franklin, 2013: Atlantic hurricane database uncertainty and presentation of a new database format. *Mon. Wea. Rev.*, **141**, 3576–3592, doi:10.1175/MWR-D-12-00254.1.

Magnan, S. G., 1998: Calculating tropical cyclone critical wind radii and storm size using NSCAT winds. M.S. thesis, Naval Postgraduate School, 55 pp. [Available online at http://calhoun.nps.edu/bitstream/handle/10945/8044/calculatingtropi00magn.pdf?sequence=1&isAllowed=y.]

Marchok, T. P., 2002: How the NCEP tropical cyclone tracker works. Preprints, *25th Conf. on Hurricanes and Tropical Meteorology*, San Diego, CA, Amer. Meteor. Soc., P1.13. [Available online at https://ams.confex.com/ams/pdfpapers/37628.pdf.]

——, M. Morin, and M. Bender, 2012: Evaluation of a GFDL hurricane model ensemble forecast system. *30th Conf. on Hurricanes and Tropical Meteorology*, Ponte Verde, FL, Amer. Meteor. Soc., 13A.3. [Available online at https://ams.confex.com/ams/30Hurricane/webprogram/Paper206200.html.]

Meissner, T., F. J. Wentz, and L. Ricciardulli, 2014: The emission and scattering of L-band microwave radiation from rough ocean surfaces and wind speed measurements from the Aquarius sensor. *J. Geophys. Res. Oceans*, **119**, 6499–6522, doi:10.1002/2014JC009837.

Mueller, K. J., M. DeMaria, J. A. Knaff, J. P. Kossin, and T. H. Vonder Haar, 2006: Objective estimation of tropical cyclone wind structure from infrared satellite data. *Wea. Forecasting*, **21**, 990–1005, doi:10.1175/WAF955.1.

NHC, 2016, Introduction to storm surge. National Hurricane Center/Storm Surge Unit, 5 pp. [Available online at http://www.nhc.noaa.gov/surge/surge_intro.pdf.]

Powell, M. D., and T. A. Reinhold, 2007: Tropical cyclone destructive potential by integrated kinetic energy. *Bull. Amer. Meteor. Soc.*, **88**, 513–526, doi:10.1175/BAMS-88-4-513.

Quiring, S., A. Schumacher, and S. Guikema, 2014: Incorporating hurricane forecast uncertainty into decision support applications. *Bull. Amer. Meteor. Soc.*, **95**, 47–58, doi:10.1175/BAMS-D-12-00012.1.

Reul, N., B. Chapron, E. Zabolotskikh, C. Donlon, Y. Quilfen, S. Guimbard, and J. F. Piolle, 2016: A revised L-band radiobrightness sensitivity to extreme winds under tropical cyclone: The 5 year SMOS-storm database. *Remote Sens. Environ.*, **180**, 274–291, doi:10.1016/j.rse.2016.03.011.

Ruf, C., and Coauthors, 2016: New ocean winds satellite mission to probe hurricanes and tropical convection. *Bull. Amer. Meteor. Soc.*, **97**, 385–395, doi:10.1175/BAMS-D-14-00218.1.

Sampson, C. R., and A. J. Schrader, 2000: The Automated Tropical Cyclone Forecasting System (version 3.2). *Bull. Amer. Meteor. Soc.*, **81**, 1231–1240, doi:10.1175/1520-0477(2000)081<1231:TATCFS>2.3.CO;2.

——, and J. Knaff, 2015: A consensus forecast for tropical cyclone gale wind radii. *Wea. Forecasting*, **30**, 1397–1403, doi:10.1175/WAF-D-15-0009.1.

——, J. L. Franklin, J. A. Knaff, and M. DeMaria, 2008: Experiments with a simple tropical cyclone intensity consensus. *Wea. Forecasting*, **23**, 304–312, doi:10.1175/2007WAF2007028.1.

——, P. A. Wittmann, and H. L. Tolman, 2010: Consistent tropical cyclone wind and wave forecasts for the U.S. Navy. *Wea. Forecasting*, **25**, 1293–1306, doi:10.1175/2010WAF2222376.1.

——, and Coauthors, 2012: Objective guidance for use in setting tropical cyclone conditions of readiness. *Wea. Forecasting*, **27**, 1052–1060, doi:10.1175/WAF-D-12-00008.1.

Student, 1908: The probable error of a mean. *Biometrika.* **6**, 1–25, doi:10.2307/2331554.

Tallapragada, V., and Coauthors, 2015: Hurricane Weather Research and Forecasting (HWRF) Model: 2015 scientific documentation, August 2015 – HWRF v3.7a. NCAR Developmental Testbed Center, Boulder, CO, 123 pp. [Available online at http://www.dtcenter.org/HurrWRF/users/docs/scientific_documents/HWRF_v3.7a_SD.pdf.]

Torn, R., and C. Snyder, 2012: Uncertainty of tropical cyclone best-track information. *Wea. Forecasting*, **27**, 715–729, doi:10.1175/WAF-D-11-00085.1.

Weigel, A. P., R. Knutti, M. A. Liniger, and C. Appenzeller, 2010: Risks of model weighting in multimodel climate projections. *J. Climate*, **23**, 4175–4191, doi:10.1175/2010JCLI3594.1.

Wu, C.-C., G.-Y. Lien, J.-H. Chen, and F. Zhang, 2010: Assimilation of tropical cyclone track and structure based on the ensemble Kalman filter (EnKF). *J. Atmos. Sci.*, **67**, 3806–3822, doi:10.1175/2010JAS3444.1.

Wu, L., W. Tian, Q. Liu, J. Cao, and J. A. Knaff, 2015: Implications of the observed relationship between tropical cyclone size and intensity over the western North Pacific. *J. Climate*, **28**, 9501–9506, doi:10.1175/JCLI-D-15-0628.1.